

Controlled Assembly and Disassembly of Higher-Order Peptide Nanotubes

Xiaoyue Ma, Yurong Zhao, Xiaofang Jiang, Mengchen Fan, Chunyong He, Hao Qi, Yan Wang, Dong Wang, Yubin Ke, Hai Xu, Cuixia Chen,* and Jiqian Wang*



Cite This: *ACS Appl. Mater. Interfaces* 2024, 16, 9787–9798



Read Online

ACCESS |

Metrics & More



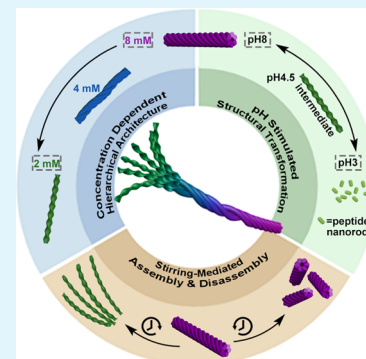
Article Recommendations



Supporting Information

ABSTRACT: The controlled peptide self-assembly and disassembly are not only implicated in many cellular processes but also possess huge application potential in a wide range of biotechnology and biomedicine. β -sheet peptide assemblies possess high kinetic stability, so it is usually hard to disassemble them rapidly. Here, we reported that both the self-assembly and disassembly of a designed short β -sheet peptide IIIGGHK could be well harnessed through the variations of concentration, pH, and mechanical stirring. Microscopic imaging, neutron scattering, and infrared spectroscopy were used to track the assembly and disassembly processes upon these stimuli, especially the interconversion between thin, left-handed protofibrils and higher-order nanotubes with superstructural right-handedness. The underlying rationale for these controlled disassembly processes mainly lies in the fact that the specific His–His interactions between protofibrils were responsive to these stimuli. By taking advantage of the peptide self-assembly and disassembly, the encapsulation of the hydrophobic drug curcumin and its rapid release upon stimuli were achieved. Additionally, the peptide hydrogels facilitated the differentiation of neural cells while maintaining low cell cytotoxicity. We believe that such dynamic and reversible structural transformation in this work provides a distinctive paradigm for controlling the peptide self-assembly and disassembly, thus laying a foundation for practical applications of peptide assemblies.

KEYWORDS: *short peptide, self-assembly, disassembly, responsiveness, His–His interactions*



INTRODUCTION

Since the serendipitous discovery of a self-assembling segment EAK16 by Zhang from a yeast protein (zuotin),¹ and the clever design of a cyclic peptide comprising alternating D and L amino acids by Ghadiri,² the self-assembly of peptides has received tremendous attention over the past 30 years. A rich variety of nanostructures have been generated through peptide self-assembly, and these nanostructures and derived materials display versatile and intriguing properties, thus imparting their huge application potential in a wide range of fields. As a typical example, the self-assembled hydrogel from RADA16, akin to EAK16, has been commercially available as PuraMatrix as a three-dimensional (3D) nanofiber scaffold for tissue engineering and regenerative medicine.^{3–5} Tao et al. have recently evaluated the application potential of peptide assemblies as semiconductors due to their unique photoactive properties.^{6,7} Additionally, short peptides can act as minimalist building blocks of long polypeptides and large proteins, whose self-assembly is usually hard to harness *in vitro*, and their self-assembly behaviors can provide an insightful understanding of the folding and misfolding of these biomacromolecules. For example, the self-assembly research of key short fragments of some amyloid peptides (*e.g.*, KLVFFAE and NFGILSS) has greatly advanced the mechanistic understanding of amyloid

fibril formation and even facilitated the development of their inhibitory agents.^{8,9}

Similar to natural protein architectures, the formation of peptide assemblies is also a hierarchical process and is tightly regulated by biological cues and environmental stimuli. As a result, many physical and biological factors have been successfully used to either trigger peptide self-assembly or prompt the sol–gel transition of peptide self-assembly. For example, Schneider and Pochan et al. have applied the variations of pH, temperature, and ionic strength to trigger the folding and subsequent self-assembly of designed hairpin peptides,^{10–12} and the research group of Xu has exploited endogenous enzymes overexpressed by bacterial and cancer cells to instruct intracellular peptide self-assembly to form nanofibers, thereby inducing cell death.^{13–16} For another example, our group has taken advantage of the enzymatic oxidation of lysine residues to convert short nanorods and micelles into long entangled nanofibers and thus induce the

Received: November 21, 2023

Revised: January 20, 2024

Accepted: January 29, 2024

Published: February 13, 2024



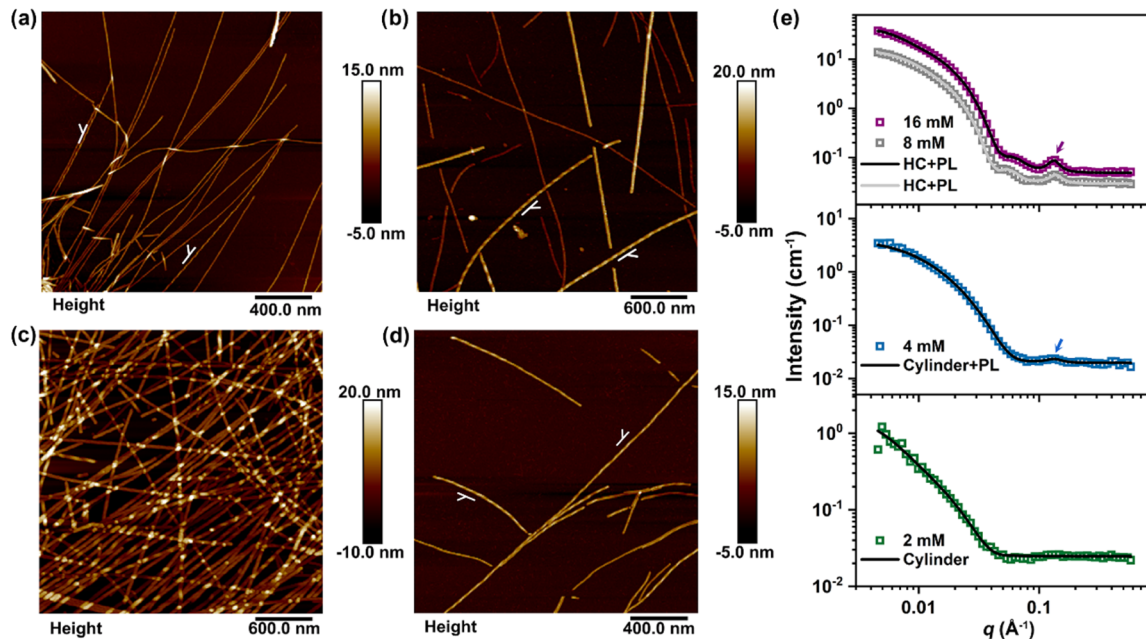


Figure 1. Concentration-mediated assembly and disassembly of IIIGGHK at pH or pD 8.0. (a–c) AFM height images of IIIGGHK assemblies formed at 2, 4, and 16 mM, respectively. (d) AFM height image of IIIGGHK assemblies immediately observed after diluting a 16 mM IIIGGHK solution to a concentration of 2 mM. The handedness of twisted/helical nanofibrils is indicated by white labels in panels (a, b, d). (e) SANS data and fitted profiles (solid lines) at 2, 4, and 16 mM. The blue and purple arrows in panel (e) denote the Bragg peaks. The key structural parameters extracted from the SANS data fitting are given in Table S1. Unless otherwise specified, the peptide solutions were incubated for 1 week at room temperature prior to characterization or further treatments.

sol–gel transition of the A_9K_2 solution, finally generating peptide hydrogels with highly selective antibacterial activities.¹⁷ In contrast, the disassembly of peptide assemblies is less explored, and their controlled disassembly upon stimuli for targeted applications remains a formidable challenge despite its specific roles in some cellular processes (e.g., actin and microtubule disassembly for cell motility and morphogenesis) and potential significances to practical applications (e.g., drug delivery and release). Such a shortcoming is virtually related to the fact that the majority of self-assembling peptides adopt β -sheet conformations and are highly hydrophobic, which makes their assemblies have a high kinetic stability. Once formed, it is usually hard to disassemble these β -sheet assemblies rapidly.¹⁸

To circumvent this dilemma, it is highly desired to develop more self-assembling peptide building blocks whose disassembly can be controlled and rapid. Peptide assemblies with a distinct hierarchy are most likely to meet these requirements. In other words, different noncovalent interactions play distinctive roles in driving their self-assembly and come into play at different levels of hierarchy, thus greatly reducing their coupling and increasing our level of control over specific assembly and disassembly processes. We have recently designed a short amphiphilic peptide IIIGGHK and demonstrated that the peptide underwent two distinct stages to form higher-order nanotubes at pH 8.0.¹⁹ Driven by backbone H-bonding and Ile side-chain hydrophobic interactions, the peptide first self-assembled into thin and left-handed protofibrils, and at the second stage, the directional His side-chain interactions including specific H-bonding and His–His pairing directed the ordered packing of protofibrils into superstructural nanotubes with right-handedness. Thus, the self-assembly of IIIGGHK is obviously different from that of amyloid and amyloid-like fibrils, in which strong hydrophobic side-chain interactions between β -sheets lead to a high level of

structural polymorphism and stability. Furthermore, the His–His interactions are most likely to be highly tunable due to the specific physiochemical properties of the imidazole ring. In light of these results and considerations, we envisage that IIIGGHK can serve as an appropriate peptide building block for controlled assembly and disassembly. In this work, we demonstrated that the assembly and disassembly processes of higher-order IIIGGHK nanotubes were well manipulated by the changes in concentration, pH, and stirring. The underlying mechanism for the disassembly process was revealed to be the destabilization of the specific His–His interactions under these stimuli. More importantly, we encapsulated the hydrophobic drug curcumin and directed its release upon stimuli by taking advantage of the peptide assembly and disassembly, respectively. Additionally, the hierarchically self-assembled IIIGGHK hydrogels were found to facilitate the differentiation of neural cells with low cell cytotoxicity, presumably due to the contribution of the active motif GHK.

RESULTS AND DISCUSSION

Concentration-Mediated Assembly and Disassembly.

First of all, we found that the assembly and disassembly of higher-order IIIGGHK nanotubes were highly concentration-dependent. At a lower concentration of 2 mM and pH 8.0, only flat and twisted thin protofibrils were observed in atomic force microscopy (AFM) imaging (Figure 1a), and the twisted ones showed left-handedness with heights fluctuating mostly between 5 and 8 nm and a relatively uniform pitch of \sim 60 nm (Figure S1a). Complementary small-angle neutron scattering (SANS) measurements confirmed this fibril morphology. As shown in Figure 1e, the measured SANS data at 2 mM can be adequately described by a Cyl model, yielding a radius of \sim 5.5 nm (black line in the bottom panel of Figure 1e, with the optimal structural parameters given in

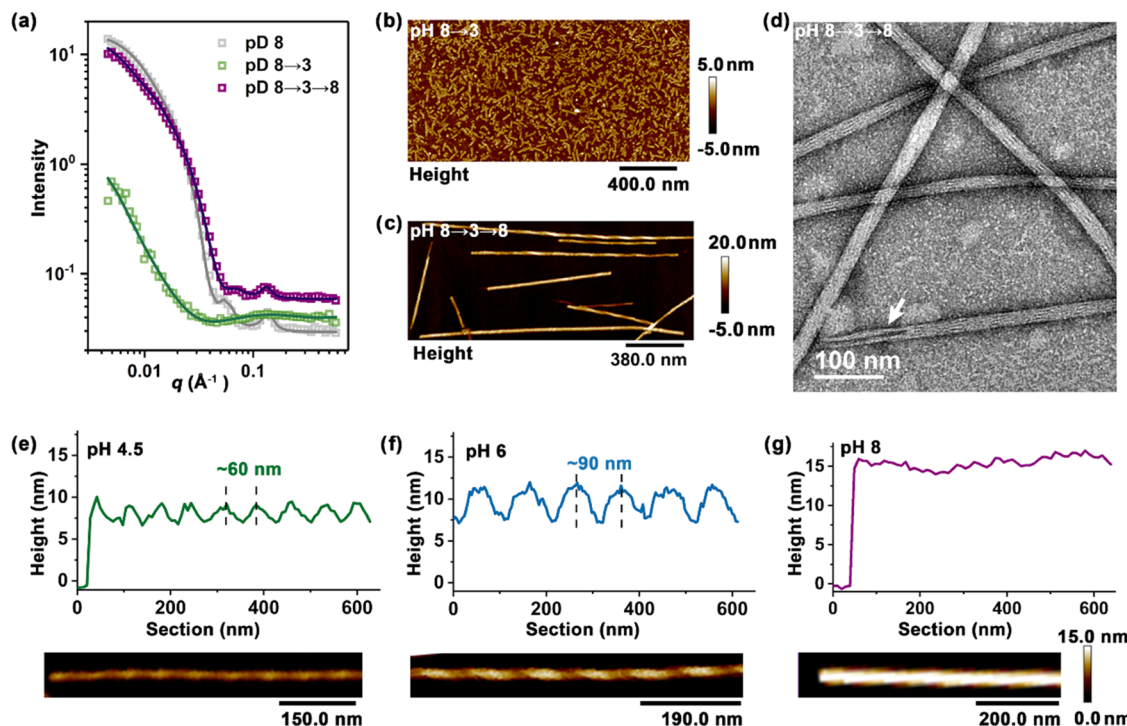


Figure 2. pH or pD-mediated assembly and disassembly of 8 mM IIIGGHK. (a) SANS data with the pD variation and fitted profiles (solid lines). SANS measurements (round 1) were first performed with the peptide solution aged for 1 week at pD 8.0 (D_2O rather than H_2O was used as the solvent for highlighting the SANS signals from the peptide). After the solution pD was lowered from 8.0 to 3.0, round 2 of SANS measurements was immediately performed. When the solution pD was adjusted back to 8.0 and further aged for 2 days, the third round of SANS measurements was performed. The key structural parameters extracted from these SANS data are given in Table S2. AFM height images of IIIGGHK assemblies (b) at ~2 h after adjusting the solution pH from 8.0 to 3.0 and (c) after 2 days when the solution pH was readjusted back to 8.0. (d) TEM micrograph of IIIGGHK nanotubes after 1 week when the solution pH was readjusted back to 8.0. AFM height images of 8 mM IIIGGHK assemblies directly prepared at (e) pH 4.5, (f) 6.0, and (g) 8.0 after incubation for 1 week. The corresponding height profiles along their longitudinal axes are also given in (e–g).

Table S1. Note that for soft peptide fibrils or tubes, their AFM heights are usually lower than their diameters derived from *in situ* SANS measurements due to the flattening effect induced by the sample dryness and substrate interference in AFM imaging. Additionally, there was no noticeable oscillation peak at q values larger than 0.1 Å⁻¹, being indicative of a lack of ordered interactions between these thin protofibrils at this lower concentration.¹⁹

With increasing peptide concentration to 4 mM, AFM measurements indicated the formation of a few thicker and helical nanofibrils (AFM heights up to ~13 nm), in addition to thin protofibrils (AFM heights: ~7 nm, Figures 1b and S1b). Importantly, these helical nanofibrils were right-handed rather than left-handed. Further, SANS measurements showed a weak peak at q of ~0.13 Å⁻¹ (indicated by the blue arrow in the middle panel of Figure 1e), suggesting the occurrence of higher-order packing. As a result, the combination of a Cyl model and a Lorentzian peak (PL) model was found to be adequate to describe the SANS data measured at 4 mM, giving rise to a fibril radius of ~5.8 nm and a Bragg peak at 0.133 Å⁻¹ with a half-width at half-maximum (HWHM) of 0.025 Å⁻¹ (the black line in the middle panel of Figure 1e, with the optimal structural parameters given in Table S1). Because SANS measurements were undertaken in solution *in situ* and the structural parameters of nanoobjects were determined with statistical significance, the slight increase in fibril radius with concentration indicated that thin protofibrils were still the dominant assemblies formed at 4 mM. The thicker and right-

handed nanofibrils observed from AFM and the Bragg peak occurred in SANS measurements, indicating the onset of association of thin protofibrils into higher-order architectures at this intermediate concentration *via* a right-handed winding mode.¹⁹ Given Bragg's Law, $d = 2\pi/q$, the center-to-center distance (d) between interacting protofibrils can be determined to be 4.72 nm.^{19,20}

At a higher concentration of 16 mM, thicker and smooth nanofibrils with heights of ~13 nm were extensively observed in AFM imaging (Figures 1c and S1c), and SANS measurements confirmed their tubular feature (the upper panel of Figure 1e), as featured by an oscillation peak at q of ~0.06 Å⁻¹, in addition to a Bragg peak at q of 0.132 Å⁻¹ (denoted by the purple arrow). Model fitting indicated that the combination of a hollow cylinder (HC) model and a PL model adequately described the SANS scattering data, giving rise to a wall thickness of ~6.8 nm and an inner radius of ~0.8 nm (the black line in the upper panel of Figure 1e, with the optimal structural parameters given in Table S1). Because the nanotube wall arose from the lateral packing of thin protofibrils,¹⁹ the wall thickness should be close to their diameters. Compared to the diameters of the thin protofibrils formed at 2 and 4 mM, however, the wall thickness increased slightly. Such an increase may be attributed to a small deformation of protofibrils upon association as well as wall curving. Complementary transmission electron microscopy (TEM) measurements revealed surface stripes along the contour length of these nanotubes as an indicator of lateral

association of thin protofibrils (Figure S2). Note that these stripes could not be observed in AFM imaging due to tip convolution. The SANS data collected at 8 mM are also given in Figure 1e as a reference, and aside from the signal intensity, the whole profile was nearly identical in shape to those at 16 mM.

When IIIGGHK solutions prepared at higher concentrations, such as 8 and 16 mM, were diluted with water to 2 mM (pH 8.0), thin nanofibrils instead of thick and closed nanotubes were widely observed immediately after dilution (Figure 1d), suggesting their rapid dissociation into their precursors, *i.e.*, protofibrils. Further, as shown in Figure S1d, most of these fibrils were left-handed twisted, though they generally showed slightly larger heights (fluctuating between 7 and 10.5 nm) and longer pitches (\sim 80 nm) compared to those directly formed at 2 mM. The dilution-induced structural transition from nanotubes to nanofibrils verified the reduction of lateral adhesion interactions, whose strength is positively correlated with the peptide monomer concentration in a certain range.^{21,22}

pH-Mediated Assembly and Disassembly. pH titrations indicated two pK_a values at 4.5 and 8.8 for an 8 mM IIIGGHK solution, corresponding to the His and Lys side chains, respectively (Figure S3a). At pH 8.0, the side-chain imidazole group of His was hence 100% deprotonated (Figure S3b), thereby favoring multiple His side-chain attractive interactions such as H-bonding and His–His pairing and eventually promoting the formation of higher-order IIIGGHK nanotubes. Because these interactions are highly dependent on the protonated state of the imidazole group, we here expected the pH-responsive assembly and disassembly of IIIGGHK nanotubes.

We applied SANS to *in situ* track changes in self-assembled nanostructures with pH, and for highlighting SANS signals from peptide, D_2O instead of H_2O was used as the solvent. After incubation for 1 week, an 8 mM solution of IIIGGHK prepared at pD 8.0 was used to serve as the starting solution, with its SANS profile (round 1) given in Figure 2a. When the pD of the starting solution was lowered from 8.0 to 3.0 using D_2O diluted DCl, this was immediately followed by the second round of SANS measurements. Note that one SANS run typically took about 2 h in our work. As shown in Figure 2a, the SANS profile collected at pD 3.0 not only showed a substantial decrease in scattering intensity but also exhibited significant variation in shape compared to that of the starting solution (pD 8.0). These results implied a rapid disassembly and significant changes in self-assembled nanostructures with such a pD variation. Consistent with this point, a single cylinder (Cyl) model, instead of the combination of an HC model and a PL model, was found to adequately describe these SANS data collected at pD 3.0, yielding a radius of \sim 8.4 nm (the green line in Figure 2a, with the optimal structural parameters given in Table S2). Note that in such a model-fitting process, this radius is always accompanied by large $\sigma/\langle \text{radius} \rangle$ values of ≥ 0.5 , suggesting its high polydispersity, possibly arising from its dynamic nature during disassembly. After the second round of SANS measurements, the solution pD was immediately adjusted back to 8.0 using D_2O diluted NaOD, followed by further incubation for 2 days and the third round of SANS measurements. As shown in Figure 2a, not only did the scattering signals restore the initial level in intensity, but also the characteristic oscillation peaks for nanotubes and higher-order interactions reoccurred, being

indicative of the reassembly of higher-order architectures. Correspondingly, the combination of an HC model and a PL model could well describe the experimental data, giving rise to a wall thickness of \sim 6.0 nm, an inner radius of \sim 0.7 nm, and a Bragg peak at 0.132 \AA^{-1} (the black line in Figure 2a, with the optimal structural parameters given in Table S2). These key structural parameters virtually varied slightly compared to those for the starting solution (a wall thickness of \sim 6.5 nm, an inner radius of \sim 0.9 nm, and a Bragg peak at 0.135 \AA^{-1} ; the gray line in Figure 2a and data in Table S2).

Microscopy characterizations also confirmed the disassembly and reassembly processes described above. As shown in Figure 2b, short nanorods were widely observed using AFM at \sim 2 h after the pH of 8 mM IIIGGHK solutions was decreased from 8.0 to 3.0. When the pH value was readjusted back to 8.0, many right-handed helical nanotubes and closed nanotubes were observed after further incubation for 2 days (Figure 2c). After 1 week of further incubation, TEM measurements showed two signatures of higher-order IIIGGHK nanotubes, *i.e.*, cavities at the end of assemblies (the white arrow) and plentiful stripes on their surface, as shown in Figure 2d.

In fact, after 24 h when the solution pH was lowered to 3.0, no aggregates of any kind were observed, suggesting a complete breakup of the peptide nanostructures. At the same time, we could not find any aggregates when 8 mM IIIGGHK solutions were directly prepared at pH 3.0. These results suggested little assembly ability of the peptide at pH 3.0. The underlying mechanism was related to the peptide charge state at this low pH value. The lysine side chain was 100% protonated, and the His side chain was nearly 100% protonated (Figure S3b). Therefore, strong intermolecular electrostatic repulsions would keep the peptide from self-assembly, and there were not multiple His–His attractive interactions at pH 3.0. However, thin and left-handed twisted protofibrils were widely observed in AFM imaging for the 8 mM IIIGGHK solution directly prepared at pH 4.5 (Figures 2e and S4a). Their AFM heights fluctuated between 6 and 9 nm, and pitches were \sim 60 nm (the upper panel of Figure 2e). At this pH value, the His side chain was 50% protonated, and half of IIIGGHK molecules were estimated to carry a single positive charge, which was from the Lys side chain (Figure S3b). Therefore, these thin and left-handed protofibrils were most likely to be formed by IIIGGHK molecules with only their Lys side chains in the cationic form as a result of greatly reduced electrostatic repulsion between molecules. At pH 6.0, we found the formation of thicker and right-handed helical nanofibrils, with heights fluctuating between 7 and 12 nm and pitches of \sim 90 nm (Figures 2f and S4b). This can be ascribed to the fact that the His side chain was \sim 98% in the neutral form, and nearly all (\sim 98%) of IIIGGHK molecules in the solution bore a single positive charge at this pH value (Figure S3b). As such, more IIIGGHK protofibrils would preform as the precursor and driven by multiple His–His attractive interactions, their subsequent winding caused the formation of right-handed superstructures. At pH 8.0, the His side chain was fully deprotonated, and the Lys side chain became \sim 15% deprotonated (Figure S3b). Thus, intermolecular repulsive forces were further decreased, and the His–His attractive interactions between protofibrils were further increased, eventually leading to the formation of closed and smooth nanotubes at a higher level of organization (Figures 2g and S4c).

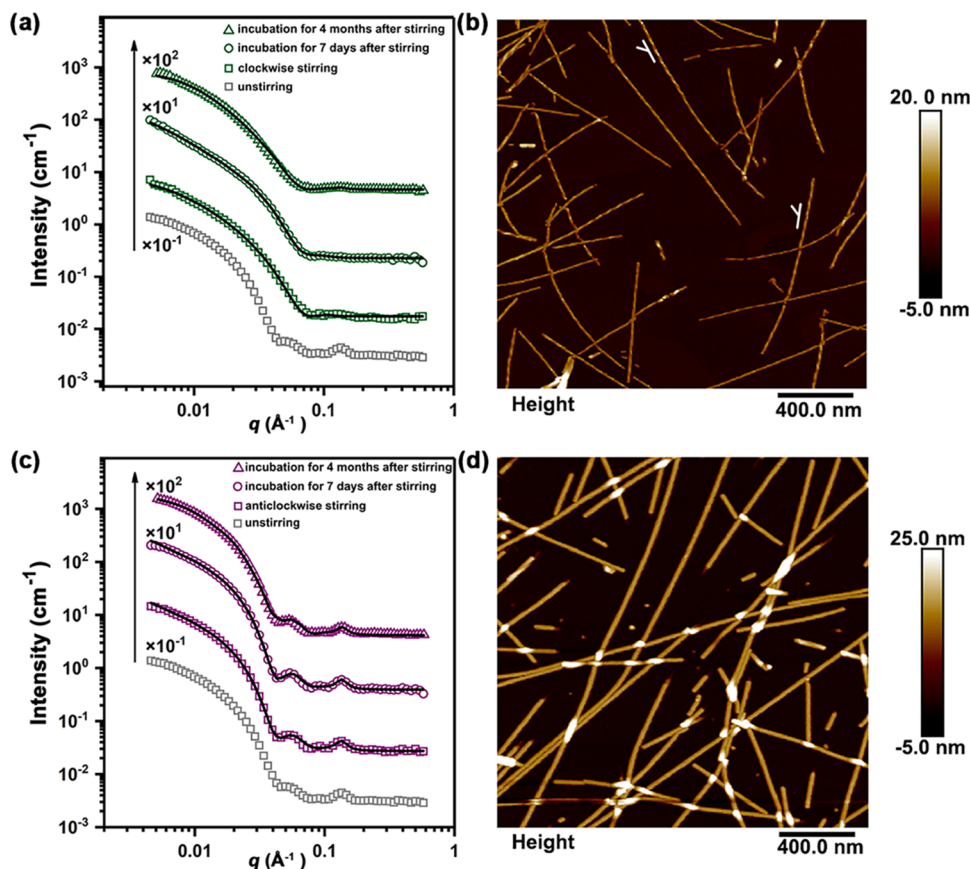


Figure 3. Stirring-mediated assembly and disassembly of IIIGGHK nanotubes formed at 8 mM and pH 8.0. (a) SANS data and fitted profiles before and after clockwise stirring. The key structural parameters extracted from the SANS data fitting are given in Table S3. (b) AFM height image after clockwise stirring. (c) SANS data and fitted profiles before and after anticlockwise stirring. The key structural parameters extracted from the SANS data fitting are given in Table S4. (d) AFM height image after anticlockwise stirring. Note that SANS measurements after stirring were performed immediately on day 7 and month 4 after 3-day stirring. AFM measurements were performed on day 7 after 3-day stirring.

Stirring-Mediated Assembly and Disassembly. Because stirring has been demonstrated to select the chirality of superstructures by exerting an asymmetric force,²³ we anticipate that stirring can tune the supramolecular assembly and chirality of IIIGGHK nanotubes. After clockwise stirring for 3 days, SANS measurements revealed the disappearance of the two oscillation peaks at q of ~ 0.055 and $\sim 0.13 \text{ \AA}^{-1}$, characteristics of nanotubes and higher-order interactions, respectively, in spite of little reduction in scattering intensity compared to the unstirred sample (Figure 3a). Correspondingly, a Cyl model was found to adequately describe the SANS data after this stirring, giving rise to a radius of $\sim 5.0 \text{ nm}$ (black lines in Figure 3a, with the optimal structural parameters given in Table S3). Complementary AFM imaging indicated the extensive occurrence of thin, left-handed twisted nanofibrils after clockwise stirring (Figure 3b), with heights fluctuating between 7 and 11 nm and pitches of $\sim 60 \text{ nm}$ (Figure S5). Because IIIGGHK nanotubes were formed through the right-handed winding of thin protofibrils, it is well understood that clockwise stirring can reverse such a process by exerting a macroscopic counter force, thereby leading to their dissociation into left-handed protofibrils. Interestingly, a conversion from these thin protofibrils back to thick nanotubes was not observed upon stirring, with the SANS profiles and fitted structural parameters being little changed with the increase of incubation time (up to 4 months) after clockwise stirring, as shown in Figure 3a and Table S3. The detailed model

explanation for this unexpected phenomenon remained to be identified in the future, and it is likely that after clockwise stirring, the orientation of His side chains along the fibril surface was significantly altered and thus sterically disfavored the specific His–His interactions (including hydrogen bonding and His–His pairing).

Conversely, because the macroscopic force exerted by anticlockwise stirring was compatible with right-handed winding, we could still observe the multilevelled IIIGGHK assemblies after such a stirring process. As shown in Figure 3c, the stirred samples showed similar SANS profiles to the unstirred sample, even with the incubation time being prolonged up to 4 months after anticlockwise stirring. Model fitting revealed that these SANS data could also be well described by the combination of an HC model and a PL model (the black lines in Figure 3c, with the optimal structural parameters given in Table S4). It is worthwhile to note that increases of $\sim 1.0\text{--}1.5 \text{ nm}$ in the wall thickness and decreases of $\sim 0.1\text{--}0.2 \text{ nm}$ in the inner radius were determined through such a model-fitting for the stirred nanotubes (Table S4) compared to the unstirred nanotubes (Table S2). These minor variations in the extracted structural parameters were consistent with the observation that the two characteristic SANS peaks became slightly more noticeable after anticlockwise stirring (Figure 3c). These results suggested an increased deformation of nanofibrils (corresponding to the nanotube wall) after anticlockwise stirring due to the additional force

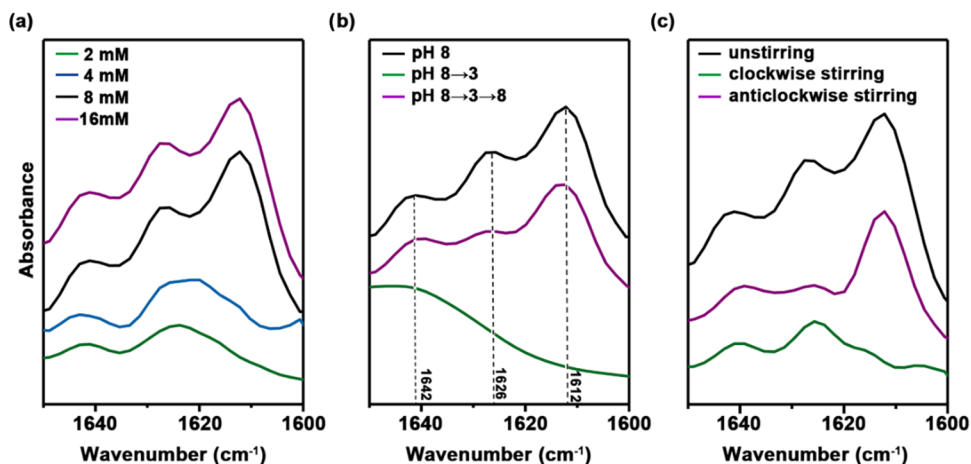


Figure 4. FTIR spectra of IIIGGHK at different (a) concentrations, (b) pH, and (c) stirring. In panel (a), IIIGGHK solutions were prepared at concentrations of 2, 4, 8, and 16 mM and pH 8.0 and subjected to FTIR measurements after incubation for 1 week. In panel (b), an 8 mM IIIGGHK solution, prepared at pH 8.0 and incubated for 1 week, acted as the control. After pH adjustment (pH 8.0 → 3.0 and pH 8.0 → 3.0 → 8.0) and further incubation for 1 day at each pH value, FTIR measurements were performed. In panel (c), an 8 mM IIIGGHK solution, prepared at pH 8.0 and incubated for 1 week, acted as the control. After clockwise or anticlockwise stirring (lasting for 3 days) and further static incubation for 1 day, FTIR measurements were performed.

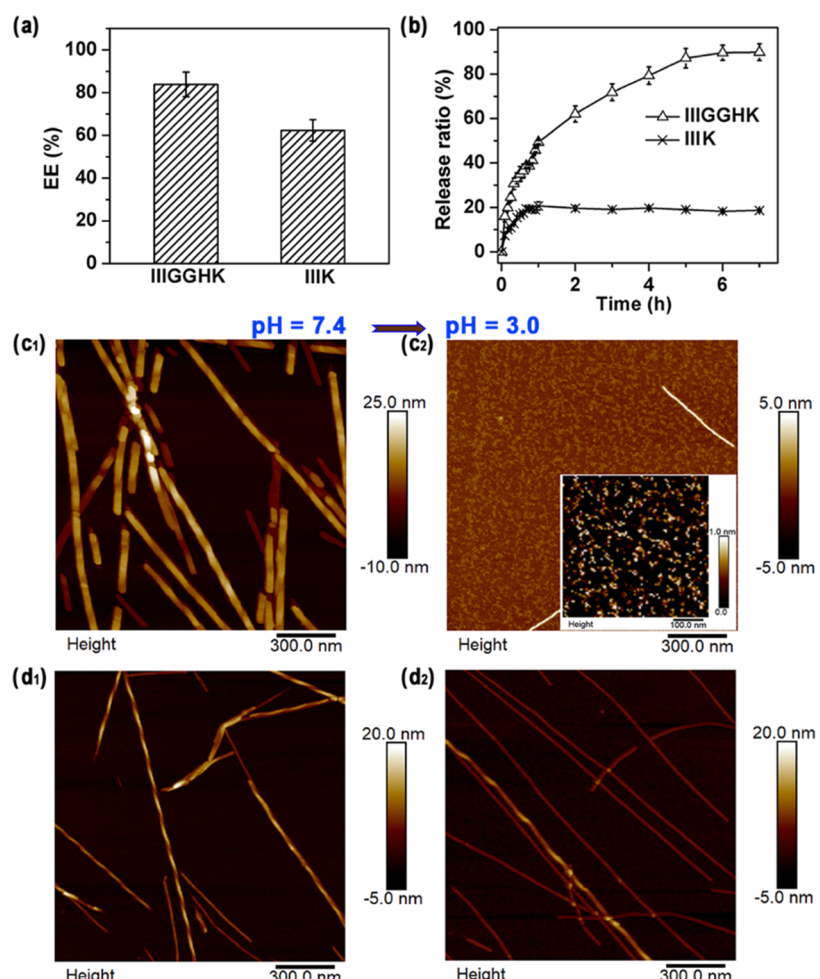


Figure 5. (a) Encapsulation efficiency (EE) of curcumin by 8 mM IIIGGHK and IIIK in an equimolar ratio. (b) Release profiles of curcumin from the coassembly systems of IIIGGHK/curcumin and IIIK/curcumin. Note that EE and release data are represented as means \pm SD ($n = 3$). (c_{1,2}) Self-assembled nanostructures of the IIIGGHK/curcumin system with a pH variation from 7.4 to 3.0. (d_{1,2}) Self-assembled nanostructures of the IIIK/curcumin system with a pH variation from 7.4 to 3.0.

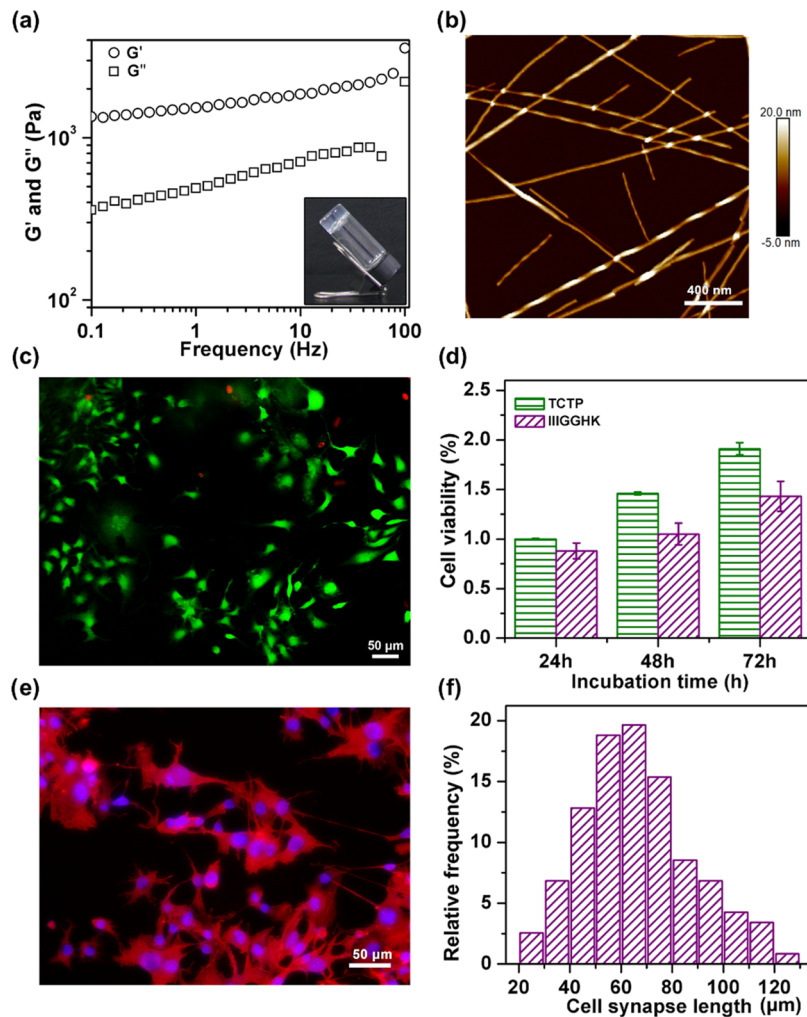


Figure 6. (a) Dynamic frequency sweep (1% strain, 25 °C) of IIIGGHK gels formed in 1× PBS (10 mM and pH 7.4) at a concentration of 4 mM, and the inset shows a self-supporting gel. (b) Self-assembled nanostructures formed by 4 mM IIIGGHK in 1× PBS. (c) Inverted fluorescence image of SH-SY5Y cells on the IIIGGHK gel surface after incubation for 3 days and live/dead staining with calcein-AM (green) and PI (red). (d) Proliferation rates of SH-SY5Y cells on the peptide gel and TCTP plate, respectively, as determined by the MTT assay. (e) Morphology of SH-SY5Y cells on the IIIGGHK gel surface after incubation for 7 days and staining with TRITC-phalloidin (red) and DAPI (blue). (f) Neurite length distribution of SH-SY5Y cells after 7 days of culture on the IIIGGHK gel surface.

exerted on right-handed winding. Complementary AFM measurements indicated the preservation of smooth nanotubes after anticlockwise stirring, although some short nanotubes occurred due to the interference of mechanical stirring (Figure 3d).

The simultaneous destabilization of different noncovalent interactions, which were responsible for distinct assembly stages, caused the disassembly of higher-order architectures into smaller aggregates or the coexistence of several components. When IIIGGHK nanotubes were disassembled into structurally independent left-handed nanofibers based on the above three stimuli, the structural transition between nanotubes and nanofibers was definitely accompanied by the changes of His–His interactions. Although other factors, such as temperature and metal ions, could also affect the IIIGGHK self-assembly, as revealed in Figures S6 and S7, the disassembly processes of peptide nanotubes were more orderly regulated by concentration, pH, and stirring, which more targeted toward the His–His interactions.

Secondary Structures. The above disassembly and reversible assembly were further elucidated by Fourier

transform infrared spectrometry (FTIR) measurements at the molecular level. As a very hydrophobic and β -branching amino acid, Ile is particularly favorable for β -sheet structuring.²⁴ We have demonstrated that higher-order IIIGGHK nanotubes displayed three characteristic FTIR peaks at ~1612, ~1626, and ~1642 cm⁻¹, respectively.¹⁹ The peak at ~1626 cm⁻¹ is ascribed to thin and left-handed β -sheet protofibrils, mainly contributing from the extended III segment; the peak at ~1612 cm⁻¹ results from the higher-order packing of β -sheet protofibrils, which is directed by the specific His–His interactions; and the one at ~1642 cm⁻¹ is attributed to random conformations, mainly arising from the flexible GGHK segment.

As shown in Figure 4, the changes of these characteristic FTIR peaks with concentration, pH, and stirring were in good line with the morphological variations observed via AFM and SANS measurements. Specifically, there was always a strong peak at ~1612 cm⁻¹ with the assembly of higher-order nanotubes, no matter whether they were reassembled via pH adjustment (Figure 4b) or underwent anticlockwise stirring (Figure 4c). However, when these higher-order nanotubes

transformed into thin and left-handed protofibrils via clockwise stirring or for the thin protofibril formed at a low concentration of 2 mM, no such absorption was observed, and there were only two peaks at \sim 1626 and \sim 1642 cm^{-1} (Figure 4a,c) instead. When the nanotubes were completely disrupted at pH 3.0, only the peak at \sim 1642 cm^{-1} , characteristic of random coils, was observable (Figure 4b).

pH-Controlled Disassembly and Curcumin Release.

To exploit the possible applications of the higher-order IIIGGHK assemblies, we encapsulated curcumin into IIIGGHK assemblies and explored the pH-controlled curcumin release behavior for its sensitive and quick structural responsiveness to pH stimuli. As a representative hydrophobic drug, curcumin has shown high application potential in combatting diverse diseases.²⁵ However, its poor solubility and rapid hydrolytic degradation in aqueous solution severely impede its clinical applications. Although many encapsulation methods or delivery vehicles have been developed, the controlled release of pharmaceutical ingredients at the site of action remains a major challenge.^{26–32} Curcumin has the ability to inhibit the growth of *Helicobacter pylori* and reduce the incidence of gastric cancers.^{33,34} Considering the extremely acidic environment in the stomach, investigating the pH-controlled curcumin release from IIIGGHK assemblies is valuable for its applications.

After mixing with curcumin at pH 7.4 in an equimolar ratio of 8 mM, IIIGGHK showed a better encapsulation effect (encapsulation efficiency (EE), \sim 84%; absolute encapsulated amount (AE), \sim 1/2.5 mg) for curcumin than its analogue IIIK (EE, \sim 62%; AE, \sim 1/2.3 mg; Figure 5a), which readily self-assembles into thin and left-handed nanofibrils rather than higher-order architecture due to the lack of additional interactions at higher scales.³⁵ As shown in Figure 5c₁, higher-order wide nanotubes with right-handedness were the dominant nanostructures assembled from the mixing of IIIGGHK and curcumin, similar to that of pure IIIGGHK. The helical nanotubes, rather than the completely closed ones formed at pH 8.0, were well expected due to the slight pH decrease. As for the comparative system of IIIK and curcumin, thin and left-handed nanofibrils were dominant in their mixing systems (Figure 5d₁). These results indicated little effect of the encapsulation of curcumin on the assembled nanostructures of the two peptides. However, it seemed that these nanostructures showed a slightly increasing in their widths, possibly due to the incorporation of substantial curcumin molecules into their hydrophobic core.

Under an acidic environment (pH 3.0), we observed a rapid release of curcumin from the mixed system of IIIGGHK and curcumin (Figure 5b). Approximately 90% of the encapsulated curcumin was released in 6 h. In contrast, after a curcumin release ratio of \sim 18% was achieved within 1 h, little release was observed for the IIIK/curcumin system with prolonged time. Compatible with these release profiles, AFM measurements at 6 h indicated that the curcumin-encapsulated IIIGGHK nanotubes completely collapsed under pH 3.0. Small micelles and very short nanorods became the dominant nanostructures instead, in addition to very few thin nanofibrils (Figure 5c₂). In contrast, thin IIIK nanofibrils still remained after this pH variation (Figure 5d₂).

Hydrogelation and Cell Culture. As an active motif, GHK plays versatile roles in tissue engineering, anticancer, and regenerative medicine.^{36,37} To assess the possibility of using the higher-order IIIGGHK assemblies as biomedical scaffolds,

we then dissolved the peptide in a phosphate-buffered saline (PBS) buffer instead of pure water. As shown in the inset of Figure 6a, a self-supporting gel formed when 4 mM peptide was dissolved in 1× PBS (10 mM and pH 7.4) for 30 min. Rheological measurements indicated that storage moduli (G') were always higher than loss storage moduli (G'') over the measured frequency of 0.1–100 Hz (Figure 6a), characteristic of viscoelastic gels. AFM imaging indicated that IIIGGHK self-assembled into thick and right-handed helical nanofibrils in a PBS solution (Figure 6b). Compared to its self-assembly in water (pH 8.0), the formation of hydrogels and the dominance of superhelical nanostructures in PBS (pH 7.4) at such a low concentration were well expected due to the greatly decreased electrostatic repulsions between molecules caused by the significantly increased solution ionic strength.

As neural cells generally do not need highly rigid matrices, we chose human neuroblastoma (SH-SY5Y) cells for cell culture. After incubation for 3 days, live/dead staining indicated that most of the cells seeded on the IIIGGHK gel exhibited green fluorescence, while a few of them displayed red fluorescence, suggesting the low cytotoxicity of the gel (Figure 6c). Simultaneously, these alive cells exhibited a spread morphology on the gel. Further MTT assay revealed a lower rate of cell proliferation on the peptide gel than on the TCTP plate (Figure 6d), implying a possible differentiation associated with the neural cells on the gel.³⁸ To confirm this hypothesis, we stained the cell cytoskeleton and nucleus with TRITC-phalloidin and DAPI, respectively. After 7 days of cell culture, the cells seeded on the peptide gel showed an obvious neuronal phenotype by extending their neurites (Figure 6e). Statistical analysis indicated that approximately 85% of the cells exhibited neurite lengths of more than 40 μm , 2–5 times as long as the cell body (Figure 6f). In contrast, although the cells on the TCTP exhibited more proliferation, they did not extend neurites (Figure S8). These results suggest a high potential of the gel as a biomedical scaffold for nerve regeneration.

CONCLUSIONS

Similar to amyloid peptides and their fragments, the majority of self-assembling peptides tend to adopt β -sheet conformations upon aggregation. Once formed, however, the β -sheet assemblies usually possess high kinetic stability and are hard to disassemble rapidly, thus limiting their practical applications. Although the designed short peptide IIIGGHK took on a β -sheet secondary structure upon self-assembly, we here demonstrated that its disassembly was well controlled by peptide concentration, solution pH, and mechanical stirring. With the increase of peptide concentration, the peptide assemblies transformed from thin, left-handed protofibrils into higher-order nanotubes through the right-handed association of protofibrils, and upon dilution to a lower concentration, a rapid disassembly of nanotubes into left-handed protofibrils was observed. As the solution pH was decreased from 8.0 to 3.0, we observed a rapid disassembly of higher-order nanotubes into short nanorods within 2 h and a complete disassembly after 24 h. When the solution pH was readjusted back to pH 8.0, the reassembly of higher-order nanotubes occurred. Because the higher-order nanotubes were formed by the association of protofibrils in a right-handed winding mode, we revealed that clockwise stirring caused the disassembly of higher-order nanotubes into left-handed protofibrils and it was interesting that upon stirring cessing,

we did not observe the reassociation of these protofibrils into higher-order nanotubes. However, anticlockwise stirring did not lead to the disassembly of higher-order nanotubes. The underlying mechanism for these controlled disassembly processes was ascribed to the destabilization or decrease of the specific His–His interactions under these stimuli. Accompanying these disassembly processes, FTIR measurements indicated the disappearance of the peak at $\sim 1612\text{ cm}^{-1}$, characteristic of higher-order packing of protofibrils.

The peptide could encapsulate the hydrophobic drug curcumin with a higher efficiency through its self-assembly at neutral pH, and the drug encapsulation had little impact on the peptide's self-assembled architecture. More importantly, a rapid and sustained release of curcumin was achieved once the solution pH was decreased to pH 3.0, which was accompanied by the disassembly of higher-order nanotubes into micelles and short nanorods. Finally, the peptide self-assembly in PBS led to the formation of hydrogels, and due to the contribution of the active motif GHK, these hydrogels facilitated the differentiation of neural cells while maintaining low cell cytotoxicity.

■ EXPERIMENTAL SECTION

Materials. The chemical materials used in peptide synthesis, including protected amino acids, Rink amide-MBHA resins, coupling reagents, and solvents, were bought from GL Biochem Ltd. (Shanghai, China) and Bo Maijie Technology (Beijing, China). Piperidine, *N,N'*-dimethylformamide (DMF), and dichloromethane (DCM) were redistilled prior to use. Hydrophobic drug curcumin, i.e., (*E,E*)-1,7-bis(4-hydroxy-3-methoxyphenyl)-1,6-heptadiene-3,5-dione, of analytical grade, calcein-AM and propidium iodide (PI), MTT dye, i.e., 3-(4,5)-dimethylthiazo(-z-y1)-3,5-diphenyltetrazoliumromide, nuclear dye DAPI (4',6-diamidino-2-phenylindole) and cytoskeleton dyes TRITC-phalloidin used in cell culture were obtained from Sigma (St. Louis, MO). All of these reagents were used as received unless otherwise specified. SH-SY5Y cells (human neuroblastoma cell line, a subclone of the parental neuroblastoma cell line SK-N-SH), purchased from the Shanghai Institute for Biological Science (Shanghai, China), were cultured in Dulbecco's modified Eagle's medium (DMEM, Gibco) with 10% heat-inactivated fetal bovine serum and maintained under a humidified 5% CO₂ atmosphere at 37 °C.

Peptide Synthesis and Solution Preparation. Peptide IIIGGHK was synthesized on a CEM Liberty microwave synthesizer based on a standard Fmoc solid-phase synthesis protocol. Detailed procedures of peptide synthesis, purification, and characterizations have been described in our previous works.^{39,40} In higher-order peptide nanotube preparation, the peptide solution of 8 mM and pH 8.0 was incubated for 2 weeks before characterizations. In the dilution regulation, the peptide concentration was diluted from 8 to 2 mM while its pH was kept at 8.0. The characterizations of the diluted samples were immediately conducted after dilution. In pH regulation, the pH was adjusted between 8.0 and 3.0. The morphology and secondary structure were characterized within a limited period (no more than 1 week) after pH adjustment. In the stirring regulation, a volume of 1 mL of peptide solution was continuously stirred clockwise or anticlockwise for 3 days at 150 rpm with a magnetic rotor (cylindrical, 3 mm × 5 mm) in a 2 mL round-bottom EP tube on a magnetic stirrer (IKA, Germany). In the temperature regulation, two parallel incubated peptide solutions were put into a water bath of 80 °C and kept for 2 and 24 h, respectively. Then, AFM observation was conducted immediately after taking the solutions out. In the experiment of metal ion regulation, copper chloride solution was added into a peptide solution of 8 mM, and the pH was readjusted to 8.0. The final Cu²⁺ concentration was 4 mM.

Morphology and Secondary Structure Characterizations. Atomic force microscopy (AFM) and transmission electron microscopy (TEM) were used to characterize the morphologies of

the peptide assemblies. AFM measurements were performed on a MultiMode 8 scanning probe microscope. An aliquot (~10 μL) of peptide solution was dropped onto a freshly cleaved mica sheet. After ~1 min of adsorption, the mica surface was gently rinsed with Milli-Q water and dried with N₂ purging. The height images were acquired in ScanAsyst mode in air and presented after first-order line fit flattening to correct the piezo-derived differences between scan lines. TEM observation was carried out on a JEOL JEM-2100 UHR transmission electron microscope with an accelerating voltage of 200 kV. In sample preparation, a volume of 5–10 μL of peptide solution was dropped on a small piece of Parafilm, and a 400 mesh copper grid coated with a carbon support film was placed on the top of the drop and kept for ~3 min for adsorption. Then, the solution adsorbed on the grid was negatively stained for ~5 min with 2% w/v uranyl acetate solution. The excess solution was removed from the edge of the copper grid by using a piece of filter paper. The Fourier transform infrared spectrometry (FTIR) spectra used to characterize secondary structures were collected at ambient temperature on a Nicolet 6700 FT-IR spectrometer equipped with a DGTS detector. Peptide solutions were prepared in D₂O for FTIR measurement. A CaF₂ sample cell with a spacer of 0.1 mm was used. 256 scans were performed at a spectral resolution of 4 cm⁻¹ for spectrum collection. The background was subtracted, and the spectra were smoothed using OMNIC software (ver. 3.0, Nicolet).

Small-Angle Neutron Scattering (SANS). SANS measurements were performed on the SANS instrument at the China Spallation Neutron Source (CSNS, Dongguan City, Guangdong Province, China). The incident neutrons with wavelengths of 1–10 Å were defined by a double-disc bandwidth chopper and collimated to the sample by a pair of apertures. The sample-to-detector distance was set to 4 m, and a sample aperture of 6 mm in diameter was used. The two-dimensional ³He tube array detector allowed a wide Q range from 0.005 to 0.70 Å⁻¹. We collected transmission and scattering data for ~10 and ~120 min for each sample, respectively. D₂O was also measured as the matrix background. The scattering data were set to absolute units after normalization, transmission correction, standard sample (50% deuterated polystyrene) calibration, and solvent background subtraction. Data fitting was performed using the SansView program (ver. 4.1.0) (<http://www.sasview.org>). Single cylinder models including a hollow cylinder (HC), cylinder (Cyl), or a combined model of cylinder and peak Lorentz (PL) model were used to fit the measured SANS data. The details of the models suitable for peptide assemblies have been given in our previous work.^{41,42}

Rheology. If 4.0 mM IIIGGHK was dissolved in 1× M PBS, it could form a self-supporting hydrogel. Its rheological property was measured with a rheometer (Haake MARS III, Thermo Scientific) in a cone–plate mode (cone angle, 2.0°, lamina diameter, 34.995 mm, truncation, 0.105 mm) at 25 °C. After the linear viscoelastic region was determined by strain sweeping from 0.1 to 100% at 1.0 Hz (Figure S9), dynamic frequency sweeps were carried out from 0.01 to 100 Hz oscillation at 1% strain.

Cell Culture. The SY5Y Cells were inoculated and cultured after thawing and 2 passages. Typically, a volume of 50 μL of cell suspension with a cell concentration of 1×10^4 cells/mL was transferred into a 96-well plate with 50 μL of peptide hydrogel (4 mM, 1× PBS) pre-overspread at the bottom of the wells. 50 μL of 1× PBS and an equal amount of cell suspension were also added as control. The half medium was changed every 2 days. After 3 days of culture, the samples were immersed in a calcein-AM (2 μM) and propidium iodide-1 (4 μM) mixed staining solution for 30 min. Then, they were washed 3 times with 1× PBS. Fluorescent images of cell morphology were collected using an inverted fluorescence microscope (DMI8, Nikon). The MTT assay was used to assess the relative density of SH-SY5Y cells qualitatively after 3 days of consecutive incubation. A volume of 20 μL of MTT (5 mg/mL in PBS) solution was added, and the cells were incubated for 4 h at 37 °C under 5% CO₂. Then, the supernatants were carefully discarded without disturbing the gel. 150 μL of dimethyl sulfoxide (DMSO) was added into each well to dissolve the formazan precipitate formed in

live cells. The absorbance at 570 nm was recorded on a microplate reader (SpectraMak Mze). After 7 days of culture, SH-SY5Y cells were fixed with 80 μ L of 4% paraformaldehyde for 30 min and then washed with 1× PBS three times. The cellular cytoskeleton was stained with 0.1% TRITC-phalloidin for 45 min at 37 °C and washed three times with 1× PBS. Then, the samples were stained with DAPI (1:1000 in 1× PBS) for 10 min at 37 °C. After 3-time rinses with 1× PBS, the samples were observed under an inverted fluorescence microscope. The average neurite length of differentiated SH-SY5Y cells was measured with ImageJ.

Drug Encapsulation and Release. IIIGGHK was mixed with equimolar curcumin in 1 mL of aqueous solution (both were 8.0 mM, pH 7.4). After 5 min vortex and 30 min ultrasound treatment, the solution was incubated under darkness for 1 week. Excess curcumin was collected through centrifugation (9168 g, 10 min) and dissolved in DMSO, and the absorption at 430 nm was determined by UV-vis absorption spectra.²⁷ The drug encapsulation efficiency (EE) was calculated by the following equation:²⁸

$$\text{EE (\%)} = \frac{m_c}{m_0} \times 100 \quad (1)$$

where m_c and m_0 represent the amount of encapsulated curcumin in the peptide assemblies and the total amount of curcumin added. In addition, the absolute encapsulated amount (AE) of curcumin was expressed as the mass ratio of encapsulated drugs to peptides (mg/mg).

The release profiles of curcumin from the peptide assemblies were measured in a modified sustained-release medium according to a reported method.²⁷ A volume of 200 μ L of peptide-curcumin solution was pipetted into a dialysis bag (M_w cutoff 3 kDa, dialysis area 2 cm²) and put into a release media of 50 mL of aqueous solution (pH 3.0) containing 20% (v/v) DMSO. The dialysate was magnetically stirred at ambient temperature. At the set time intervals, 800 μ L of medium was taken out for absorbance detection at 430 nm, and the sampled solution was returned to the dialysis beaker after testing. The accumulative release ratio (RR) of the peptide assemblies was calculated as follows:^{27,28,43}

$$\text{RR (\%)} = \frac{m_r}{m_c} \times 100 \quad (2)$$

where m_r and m_c are the amounts of released curcumin (milligrams) and encapsulated curcumin (mg), respectively. All results were the average of three tests, and the data were expressed with standard deviation in the release profiles.

ASSOCIATED CONTENT

Supporting Information

The Supporting Information is available free of charge at <https://pubs.acs.org/doi/10.1021/acsami.3c17509>.

AFM height profiles of IIIGGHK assemblies at different concentrations; TEM image of IIIGGHK assemblies at 16 mM; pH titration curve and charge state of IIIGGHK; AFM height images of IIIGGHK assemblies directly prepared at different pH values; AFM height image and height profile of IIIGGHK assemblies after clockwise stirring; heating- and Cu²⁺-mediated disassembly; morphology of SH-SY5Y cells on the TCTP; and the fitting models and optimal structural parameters extracted from SANS data (PDF)

AUTHOR INFORMATION

Corresponding Authors

Cuixia Chen – State Key Laboratory of Heavy Oil Processing and Department of Biological and Energy Chemical Engineering, China University of Petroleum (East China),

Qingdao 266580, China; orcid.org/0000-0003-3168-2238; Email: chencx@upc.edu.cn

Jiqian Wang – State Key Laboratory of Heavy Oil Processing and Department of Biological and Energy Chemical Engineering, China University of Petroleum (East China), Qingdao 266580, China; orcid.org/0000-0002-7525-5943; Email: jqwang@upc.edu.cn

Authors

Xiaoyue Ma – State Key Laboratory of Heavy Oil Processing and Department of Biological and Energy Chemical Engineering, China University of Petroleum (East China), Qingdao 266580, China

Yurong Zhao – State Key Laboratory of Heavy Oil Processing and Department of Biological and Energy Chemical Engineering, China University of Petroleum (East China), Qingdao 266580, China; orcid.org/0000-0002-3727-158X

Xiaofang Jiang – State Key Laboratory of Heavy Oil Processing and Department of Biological and Energy Chemical Engineering, China University of Petroleum (East China), Qingdao 266580, China

Mengchen Fan – State Key Laboratory of Heavy Oil Processing and Department of Biological and Energy Chemical Engineering, China University of Petroleum (East China), Qingdao 266580, China

Chunyong He – Dongguan Neutron Source Science Center, Dalang, Dongguan 523803, China; Institute of High Energy Physics, Chinese Academy of Sciences (CAS), Beijing 100049, China; orcid.org/0000-0002-6045-3648

Hao Qi – State Key Laboratory of Heavy Oil Processing and Department of Biological and Energy Chemical Engineering, China University of Petroleum (East China), Qingdao 266580, China

Yan Wang – State Key Laboratory of Heavy Oil Processing and Department of Biological and Energy Chemical Engineering, China University of Petroleum (East China), Qingdao 266580, China

Dong Wang – State Key Laboratory of Heavy Oil Processing and Department of Biological and Energy Chemical Engineering, China University of Petroleum (East China), Qingdao 266580, China; orcid.org/0000-0002-2361-6647

Yubin Ke – Dongguan Neutron Source Science Center, Dalang, Dongguan 523803, China; Institute of High Energy Physics, Chinese Academy of Sciences (CAS), Beijing 100049, China

Hai Xu – State Key Laboratory of Heavy Oil Processing and Department of Biological and Energy Chemical Engineering, China University of Petroleum (East China), Qingdao 266580, China; orcid.org/0000-0002-5796-4404

Complete contact information is available at:

<https://pubs.acs.org/doi/10.1021/acsami.3c17509>

Author Contributions

X.M., H.X., and J.W. conceived the project, X.M., C.C., Y.W., and H.X. designed and synthesized the peptides, Y.Z., X.J., M.F., H.Q., Y.W., and D.W. carried out AFM, TEM, and CD measurements, H.Q., C.H., Y.K., and H.X. performed SANS measurements and corresponding data fitting, and X.M., Y.Z., X.J., J.W., C.C., and H.X. analyzed the data and wrote the manuscript. All authors discussed the results and reviewed the manuscript.

Notes

The authors declare no competing financial interest.

ACKNOWLEDGMENTS

This work was supported by the National Natural Science Foundation of China under grant numbers 22072181, 22172193, and U1832108. We acknowledge the use of the resources of the China Spallation Neutron Source in Dongguan of Guangdong Province of P. R. China.

REFERENCES

- (1) Zhang, S.; Holmes, T.; Lockshin, C.; Rich, A. Spontaneous Assembly of a Self-Complementary Oligopeptide to Form a Stable Macroscopic Membrane. *Proc. Natl. Acad. Sci. U.S.A.* **1993**, *90* (8), 3334–3338.
- (2) Ghadiri, M. R.; Granja, J. R.; Milligan, R. A.; McRee, D. E.; Khazanovich, N. Self-Assembling Organic Nanotubes Based on a Cyclic Peptide Architecture. *Nature* **1993**, *366* (6453), 324–327.
- (3) Loo, Y.; Zhang, S.; Hauser, C. A. E. From Short Peptides to Nanofibers to Macromolecular Assemblies in Biomedicine. *Biotechnol. Adv.* **2012**, *30* (3), 593–603.
- (4) Yang, Z.; Xu, H.; Zhao, X. Designer Self-Assembling Peptide Hydrogels to Engineer 3D Cell Microenvironments for Cell Constructs Formation and Precise Oncology Remodeling in Ovarian Cancer. *Adv. Sci.* **2020**, *7* (9), No. 1903718.
- (5) <https://www.3d-matrix.co.jp/en/product/pro2.html>.
- (6) Tao, K.; Makam, P.; Aizen, R.; Gazit, E. Self-Assembling Peptide Semiconductors. *Science* **2017**, *358* (6365), No. eaam9756.
- (7) Sun, B.; Tao, K.; Jia, Y.; Yan, X.; Zou, Q.; Gazit, E.; Li, J. Photoactive Properties of Supramolecular Assembled Short Peptides. *Chem. Soc. Rev.* **2019**, *48* (16), 4387–4400.
- (8) Porat, Y.; Mazor, Y.; Efrat, S.; Gazit, E. Inhibition of Islet Amyloid Polypeptide Fibril Formation: A Potential Role for Heteroaromatic Interactions. *Biochemistry* **2004**, *43*, 14454–14462.
- (9) Lu, K.; Jacob, J.; Thiagarajan, P.; Conticello, V. P.; Lynn, D. G. Exploiting Amyloid Fibril Lamination for Nanotube Self-Assembly. *J. Am. Chem. Soc.* **2003**, *125* (21), 6391–6393.
- (10) Schneider, J. P.; Pochan, D. J.; Ozbas, B.; Rajagopal, K.; Pakstis, L.; Kretsinger, J. Responsive Hydrogels from the Intramolecular Folding and Self-Assembly of a Designed Peptide. *J. Am. Chem. Soc.* **2002**, *124* (50), 15030–15037.
- (11) Pochan, D. J.; Schneider, J. P.; Kretsinger, J.; Ozbas, B.; Rajagopal, K.; Haines, L. Thermally Reversible Hydrogels via Intramolecular Folding and Consequent Self-Assembly of a *de novo* Peptide. *J. Am. Chem. Soc.* **2003**, *125* (39), 11802–11803.
- (12) Ozbas, B.; Kretsinger, J.; Rajagopal, K.; Schneider, J. P.; Pochan, D. J. Salt-Triggered Peptide Folding and Consequent Self-Assembly into Hydrogels with Tunable Modulus. *Macromolecules* **2004**, *37* (19), 7331–7337.
- (13) Yang, Z.; Liang, G.; Guo, Z.; Guo, Z.; Xu, B. Intracellular Hydrogelation of Small Molecules Inhibits Bacterial Growth. *Angew. Chem., Int. Ed.* **2007**, *46* (43), 8216–8219.
- (14) Yang, Z. M.; Xu, K. M.; Guo, Z. H.; Guo, Z.; Xu, B. Intracellular Enzymatic Formation of Nanofibers Results in Hydrogelation and Regulated Cell Death. *Adv. Mater.* **2007**, *19* (20), 3152–3156.
- (15) Zhou, J.; Du, X.; Yagagata, N.; Xu, B. Enzyme-Instructed Self-Assembly of Small D-Peptides as a Multiple-Step Process for Selectively Killing Cancer Cells. *J. Am. Chem. Soc.* **2016**, *138* (11), 3813–3823.
- (16) Liu, S.; Zhang, Q.; Shy, A. N.; Yi, M.; He, H.; Lu, S.; Xu, B. Enzymatically Forming Intranuclear Peptide Assemblies for Selectively Killing Human Induced Pluripotent Stem Cells. *J. Am. Chem. Soc.* **2021**, *143* (38), 15852–15862.
- (17) Bai, J. K.; Chen, C. C.; Wang, J. X.; Zhang, Y.; Cox, H.; Zhang, J.; Wang, Y. M.; Penny, J.; Waigh, T.; Lu, J. R.; Xu, H. Enzymatic Regulation of Self-Assembling Peptide A₉K₂ Nanostructures and Hydrogelation with Highly Selective Antibacterial Activities. *ACS Appl. Mater. Interfaces* **2016**, *8* (24), 15093–15102.
- (18) Korevaar, P. A.; Newcomb, C.; Meijer, E. W.; Stupp, S. I. Pathway Selection in Peptide Amphiphile Assembly. *J. Am. Chem. Soc.* **2014**, *136* (24), 8540–8543.
- (19) Ma, X. Y.; Zhao, Y. R.; He, C. Y.; Zhou, X.; Qi, H.; Wang, Y.; Chen, C. X.; Wang, D.; Li, J.; Ke, Y. B.; Wang, J. Q.; Xu, H. Ordered Packing of β -Sheet Nanofibrils into Nanotubes: Multi-hierarchical Assembly of Designed Short Peptides. *Nano Lett.* **2021**, *21* (24), 10199–10207.
- (20) Cui, H.; Muraoka, T.; Cheetham, A. G.; Stupp, S. I. Self-Assembly of Giant Peptide Nanobelts. *Nano Lett.* **2009**, *9* (3), 945–951.
- (21) Nyrkova, I. A.; Semenov, A. N.; Aggeli, A.; Boden, N.; McLeish, T. C. B. Self-Assembly and Structure Transformations in Living Polymers forming Fibrils. *Eur. Phys. J. B* **2000**, *17* (3), 499–513.
- (22) Aggeli, A.; Nyrkova, I. A.; Bell, M.; Harding, R.; Carrick, L.; McLeish, T. C. B.; Semenov, A. N.; Boden, N. Hierarchical Self-Assembly of Chiral Rod-Like Molecules as a Model for Peptide β -sheet Tapes. *Proc. Natl. Acad. Sci. U.S.A.* **2001**, *98* (21), 11857–11862.
- (23) Ribó, J. M.; Crusats, J.; Sagués, F.; Claret, J.; Rubires, R. Chiral Sign Induction by Vortices During the Formation of Mesophases in Stirred Solutions. *Science* **2001**, *292* (5524), 2063–2066.
- (24) Minor, D. L. J.; Kim, P. S. Measurement of the β -Sheet-Forming Propensities of Amino Acids. *Nature* **1994**, *367* (6464), 660–663.
- (25) Kunnumakkara, A. B.; Hegde, M.; Parama, D.; Girisa, S.; Kumar, A.; Daimary, U. D.; Garodia, P.; Yenisetti, S. C.; Oommen, O. V.; Aggarwal, B. B. Role of Turmeric and Curcumin in Prevention and Treatment of Chronic Diseases: Lessons Learned from Clinical Trials. *ACS Pharmacol. Transl. Sci.* **2023**, *6* (4), 447–518.
- (26) Anand, P.; Kunnumakkara, A. B.; Newman, R. A.; Aggarwal, B. B. Bioavailability of Curcumin: Problems and Promises. *Mol. Pharmaceutics* **2007**, *4* (6), 807–818.
- (27) Li, Y.; Zou, Q.; Yuan, C.; Li, S.; Xing, R.; Yan, X. Amino Acid Coordination Driven Self-Assembly for Enhancing both the Biological Stability and Tumor Accumulation of Curcumin. *Angew. Chem., Int. Ed.* **2018**, *57* (52), 17084–17088.
- (28) Dai, Y.; Jiang, Z.; Li, J.; Wang, M.; Liu, C.; Qi, W.; Su, R.; He, Z. Co-Assembly of Curcumin and a Cystine Bridged Peptide to Construct Tumor-Responsive Nano-Micelles for Efficient Chemotherapy. *J. Mater. Chem. B* **2020**, *8* (9), 1944–1951.
- (29) Madamsetty, V. S.; Vazifehdoost, M.; Alhashemi, S. H.; Davoudi, H.; Zarrafi, A.; Dehshahri, A.; Fekri, H. S.; Mohammadinejad, R.; Thakur, V. K. K. Next-Generation Hydrogels as Biomaterials for Biomedical Applications: Exploring the Role of Curcumin. *ACS Omega* **2023**, *8* (10), 8960–8970.
- (30) Yang, J. Z.; Zhang, X. D.; Lu, B. L.; Mei, J. W.; Xu, L.; Zhang, X. Z.; Su, Z.; Xu, W.; Fang, S. Y.; Zhu, C.; Xu, D. D.; Zhu, W. B. Inflammation-Responsive Hydrogel Spray for Synergistic Prevention of Traumatic Heterotopic Ossification via Dual-Homeostatic Modulation Strategy. *Adv. Sci.* **2023**, *10* (30), No. 2302905.
- (31) Ji, C. L.; Li, H.; Zhang, L.; Wang, P.; Lv, Y. W.; Sun, Z. J.; Tan, J.; Yuan, Q.; Tan, W. H. Ferrocene-Containing Nucleic Acid-Based Energy-Storage Nanoagent for Continuously Photo-Induced Oxidative Stress Amplification. *Angew. Chem., Int. Ed.* **2022**, *61* (13), No. e202200237.
- (32) Fang, F.; Wang, S.; Song, Y. Y.; Sun, M.; Chen, W. C.; Zhao, D. X.; Zhang, J. F. Continuous Spatiotemporal Therapy of A Full-API Nanodrug via Multi-Step Tandem Endogenous Biosynthesis. *Nat. Commun.* **2023**, *14* (1), No. 1660.
- (33) De, R.; Kundu, P.; Swarnakar, S.; Ramamurthy, T.; Chowdhury, A.; Nair, G. B.; Mukhopadhyay, A. K. Antimicrobial Activity of Curcumin against *Helicobacter pylori* Isolates from India and during Infections in Mice. *Antimicrob. Agents Chemother.* **2009**, *53* (4), 1592–1597.
- (34) Mahmoud, D. B. E. D.; Marzok, S. *In situ* Supersaturable Polyhydrogels: A Feasible Modification of the Conventional Hydro-

- gels for the Enhanced Delivery of Stomach Specific Hydrophobic Drugs. *J. Drug Delivery Sci. Technol.* **2020**, *58*, No. 101744.
- (35) Wang, M.; Zhou, P.; Wang, J.; Zhao, Y.; Ma, H.; Lu, J. R.; Xu, H. Left or Right: How Does Amino Acid Chirality Affect the Handedness of Nanostructures Self-Assembled from Short Amphiphilic Peptides? *J. Am. Chem. Soc.* **2017**, *139* (11), 4185–4194.
- (36) Pickart, L. The Human Tri-Peptide GHK and Tissue Remodeling. *J. Biomater. Sci., Polym. Ed.* **2008**, *19* (8), 969–988.
- (37) Klontzas, M. E.; Reakasame, S.; Silva, R.; Morais, J. C. F.; Vernardis, S.; MacFarlane, R. J.; Heliotis, M.; Tsiridis, E.; Panoskaltsis, N.; Boccaccini, A. R.; Mantalaris, A. Oxidized Alginate Hydrogels with the GHK Peptide Enhance Cord Blood Mesenchymal Stem Cell Osteogenesis: A Paradigm for Metabolomics-Based Evaluation of Biomaterial Design. *Acta Biomater.* **2019**, *88*, 224–240.
- (38) Miloso, M.; Villa, D.; Crimi, M.; Galbiati, S.; Donzelli, E.; Nicolini, G.; Tredici, G. Retinoic Acid-Induced Neuritogenesis of Human Neuroblastoma SH-SY5Y Cells Is ERK Independent and PKC Dependent. *J. Neurosci. Res.* **2004**, *75* (2), 241–252.
- (39) Zhao, Y. R.; Yang, W.; Wang, D.; Wang, J. Q.; Li, Z.; Hu, X. Z.; King, S.; Rogers, S.; Lu, J. R.; Xu, H. Controlling the Diameters of Nanotubes Self-Assembled from Designed Peptide Bolaphiles. *Small* **2018**, *14* (12), No. 1703216.
- (40) Han, S. Y.; Cao, S. S.; Wang, Y. M.; Wang, J. Q.; Xia, D. H.; Xu, H.; Zhao, X. B.; Lu, J. R. Self-Assembly of Short Peptide Amphiphiles: the Cooperative Effect of Hydrophobic Interaction and Hydrogen Bonding. *Chem. - Eur. J.* **2011**, *17* (46), 13095–13102.
- (41) Wang, M.; Wang, J. Q.; Zhou, P.; Deng, J.; Zhao, Y. R.; Sun, Y.; Yang, W.; Wang, D.; Li, Z.; Hu, X.; King, S. M.; Rogers, S. E.; Cox, H.; Waigh, T. A.; Yang, J.; Lu, J. R.; Xu, H. Nanoribbons Self-Assembled from Short Peptides Demonstrate the Formation of Polar Zippers between β -Sheets. *Nat. Commun.* **2018**, *9*, No. 5118.
- (42) Zhao, Y. R.; Wang, J. Q.; Deng, L.; Zhou, P.; Wang, S.; Wang, Y.; Xu, H.; Lu, J. R. Tuning the Self-Assembly of Short Peptides via Sequence Variations. *Langmuir* **2013**, *29* (44), 13457–13464.
- (43) Wei, Y.; Guo, A. X.; Liu, Z. K.; Zhang, L.; Liao, W. Y.; Liu, J. F.; Mao, L. K.; Yuan, F.; Gao, Y. X. Development of Curcumin Loaded Core-Shell Zein Microparticles Stabilized by Cellulose Nanocrystals and Whey Protein Microgels through Interparticle Interactions. *Food Funct.* **2021**, *12* (15), 6936–6949.

CAS INSIGHTS™
EXPLORE THE INNOVATIONS SHAPING TOMORROW

Discover the latest scientific research and trends with CAS Insights. Subscribe for email updates on new articles, reports, and webinars at the intersection of science and innovation.

[Subscribe today](#)

CAS
A division of the
American Chemical Society